Screening and Separation of Charges in Microscale Devices: Complete Planar Solution of the Poisson−Boltzmann Equation

ARTICLE *in* THE JOURNAL OF PHYSICAL CHEMISTRY B · OCTOBER 2008

Impact Factor: 3.3 · DOI: 10.1021/jp800675w · Source: PubMed

6 AUTHORS, INCLUDING:

Peter H L Notten
Technische Universiteit Eindhoven
218 PUBLICATIONS **4,787** CITATIONS
SEE PROFILE

Filip Strubbe
Ghent University
32 PUBLICATIONS **261** CITATIONS
SEE PROFILE

Filip Beunis
Ghent University
60 PUBLICATIONS **427** CITATIONS
SEE PROFILE

Kristiaan Neyts
Ghent University
249 PUBLICATIONS **2,076** CITATIONS
SEE PROFILE

Screening and Separation of Charges in Microscale Devices: Complete Planar Solution of the Poisson−Boltzmann Equation

Alwin R. M. Verschueren,*,† Peter H. L. Notten,† Luc J. M. Schlangen,† Filip Strubbe,‡ Filip Beunis,‡ and Kristiaan Neyts‡

Philips Research Laboratories, High Tech Campus 34, 5656 AE Eindhoven, The Netherlands, and ELIS Department, Ghent University, Sint-Pietersnieuwstraat 41, B9000 Ghent, Belgium

Received: January 23, 2008; Revised Manuscript Received: April 23, 2008

The Poisson−Boltzmann (PB) equation is widely used to calculate the interaction between electric potential and the distribution of charged species. In the case of a symmetrical electrolyte in planar geometry, the Gouy−Chapman (GC) solution is generally presented as the analytical solution of the PB equation. However, we demonstrate here that this GC solution assumes the presence of a bulk region with zero electric field, which is not justified in microdevices. In order to extend the range of validity, we obtain here the complete numerical solution of the planar PB equation, supported with analytical approximations. For low applied voltages, it agrees with the GC solution. Here, the electric double layers fully absorb the applied voltage such that a region appears where the electric field is screened. For higher voltages (of order 1 V in microdevices), the solution of the PB equation shows a dramatically different behavior, in that the double layers can no longer absorb the complete applied voltage. Instead, a finite field remains throughout the device that leads to complete separation of the charged species. In this higher voltage regime, the double layer characteristics are no longer described by the usual Debye parameter κ, and the ion concentration at the electrodes is intrinsically bound (even without assuming steric interactions). In addition, we have performed measurements of the electrode polarization current on a nonaqueous model electrolyte inside a microdevice. The experimental results are fully consistent with our calculations, for the complete concentration and voltage range of interest.

1. Introduction

The Poisson−Boltzmann (PB) equation is a very important equation, as it constitutes a wide ranging fundament for our understanding of electrolyte solutions,[1] electrode processes,[2] colloid interaction,[3,4] membrane transport,[5,6] structure of biomolecules,[7,8] transistor behavior,[9] plasma discharges,[10] microfluidic pumping,[11] supercapacitors,[12] battery performance,[13] and even the durability of concrete.[14] The PB equation follows from the combined description of charges influencing the electrical potential (Poisson's equation) and vice-versa the electrical potential determining the positions of charges (the Boltzmann distribution). Despite its simple derivation and intensive use for almost 100 years, no general analytical solution is known at present. For two special subcases, analytical solutions are known and widely used: the Debye−Hückel theory[15] for small potentials and the Gouy−Chapman (GC) theory[16,17] for binary symmetric z:z electrolytes in planar geometry. However, in this paper, it will be demonstrated that the latter GC solution contains an assumption that was reasonable at the time of its inception but at present, as the dimensions of devices come into the micrometer range, may no longer be justified. The implications of this assumption are not discussed in leading textbooks[18–22] and consequently may lead to unjustified use of the GC theory in microscale devices particularly with nonaqueous solvents.

In the first part of this paper, analytical and numerical solutions are presented for a binary symmetric z:z electrolyte in a bounded planar geometry, without the assumption of the GC theory. In fact, the GC solution will naturally appear as a subset of this complete solution. The concentration and electric field profiles of the complete solution space are given, including analytical expressions for convenient estimation. From this complete solution, it will become apparent that above a sharply defined threshold voltage the electrical double layers behave completely different as in the GC theory; in fact, the opposite charges of the electrolyte will become fully separated. In the second part of this paper, the electrode polarization charge will be measured in an actual microscale device filled with nonaqueous electrolyte. These measurements fully support the presented calculations and the predicted charge separation.

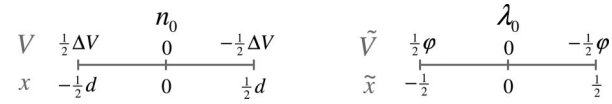

Figure 1. Diagram of parameter definitions and normalizations.

1.1. Poisson−Boltzmann Equation. The Poisson−Boltzmann equation can be derived from rigorous statistical mechanics[23] under the assumption that finite size effects, and ion−ion correlations (other than through the mean potential) can be neglected. Both assumptions are justified as long as the ion concentrations are not extremely high. In section 3 of this paper, it will be demonstrated that the full solutions presented here (supported by measurements) indeed remain in this range of validity.

To illustrate the processes that form the distribution of charges, the PB equation will now be derived in an alternative way, by first retrieving the "Nernst−Planck" equation.[24,25] Figure 1 represents a planar (1D) geometry with position

* Corresponding author. E-mail: alwin.verschueren@philips.com.
† Philips Research Laboratories.
‡ Ghent University.

10.1021/jp800675w CCC: $40.75
Published on Web 09/19/2008

coordinate x (in m), bounded by two electrodes located at $x = \pm^1/_2 d$, where d denotes the characteristic device dimension (in m). At every position x, the local migration (or drift) current density J^i_{mig} of ion species i (in A m^{-2}) under influence of the local electric field E (in V m^{-1}) is defined[20] as

$$J^i_{mig} = z^i e n^i \mu^i E \tag{1}$$

where n^i is the local concentration (in m^{-3}), z^i is the valency (in units of the electron charge $e = 1.6 \times 10^{-19}$ C), and μ^i the electrophoretic mobility (in m^2 V^{-1} s^{-1}) of ion species i. The local diffusion current density J^i_{dif} arising from concentration gradients is given by Fick's first law[20]

$$J^i_{dif} = -z^i e D^i \nabla n^i = -\mu^i kT \nabla n^i \tag{2}$$

where D^i is the diffusion constant (in m^2 s^{-1}). The right-hand side of eq 2 follows from the Einstein relation:[26] diffusion and migration processes both experience the same drag resistance in liquids, and therefore the diffusion constant D^i can be related to the electrophoretic mobility μ^i, Boltzmann constant $k = 1.38 \times 10^{-23}$ J K^{-1} and absolute temperature T (in K).

The Nernst−Planck equation defines the total current density as the sum of eq 1 and eq 2. In case no faradaic currents are present at the bounding electrodes, the steady-state migration and diffusion fluxes of all individual ionic species should balance each other, yielding at every position x

$$n^i E = \frac{kT}{z^i e} \nabla n^i \tag{3}$$

Converting the electric field into the electrostatic potential V by $E = -\nabla V$, it is possible to isolate the concentration and obtain the Boltzmann distribution

$$n^i = n^i_0 \exp\left(-\frac{z^i e V}{kT}\right) \tag{4}$$

where the subscript 0 in n^i_0 denotes the concentration of ion species i at the midplane $x = 0$ of the device where the potential V is referenced to 0. The Poisson equation describes how the ionic species affect the electric field

$$\nabla \cdot E = \frac{e}{\varepsilon_0 \varepsilon_r} \sum_i z^i n^i \tag{5}$$

with the vacuum permittivity $\varepsilon_0 = 8.85 \times 10^{-12}$ F m^{-1} and the relative permittivity ε_r of the liquid hosting the charges. The combination of eq 4 and eq 5 leads to the usual form of the PB equation for a general electrolyte

$$\nabla^2 V = -\frac{e}{\varepsilon_0 \varepsilon_r} \sum_i z^i n^i_0 \exp\left(-\frac{z^i e V}{kT}\right) \tag{6}$$

In this work, we focus on a binary symmetric z:z electrolyte defined as $n^+_0 = n^-_0 = n_0$ and $z^+ = -z^- = z$, for which eq 6 simplifies to

$$\nabla^2 V = \frac{2 z e n_0}{\varepsilon_0 \varepsilon_r} \sinh\left(\frac{zeV}{kT}\right) \tag{7}$$

Converting this equation into its dimensionless planar form gives

$$\frac{\partial^2 \tilde{V}}{\partial \tilde{x}^2} = \lambda_0 \sinh(\tilde{V}) \qquad \tilde{V} \equiv \frac{zeV}{kT} \qquad \lambda_0 \equiv \frac{2 n_0 z^2 e^2 d^2}{\varepsilon_0 \varepsilon_r kT} \tag{8}$$

where dimensionless position $\tilde{x} = x/d$, dimensionless voltage $\tilde{V}$ and dimensionless concentration (at the midplane) λ_0 are used. At this midplane $\tilde{x} = 0$, we define the zero reference of the potential $\tilde{V} = 0$, and because of the symmetry in eq 8, the potentials at both ends of the device will become opposite (equal to $\pm^1/_2 \varphi$; see Figure 1). Notice that recently published analytical approximations[27] of the PB equation do not apply here, as instead of a symmetrical electrolyte only ions of single polarity were taken into account there.

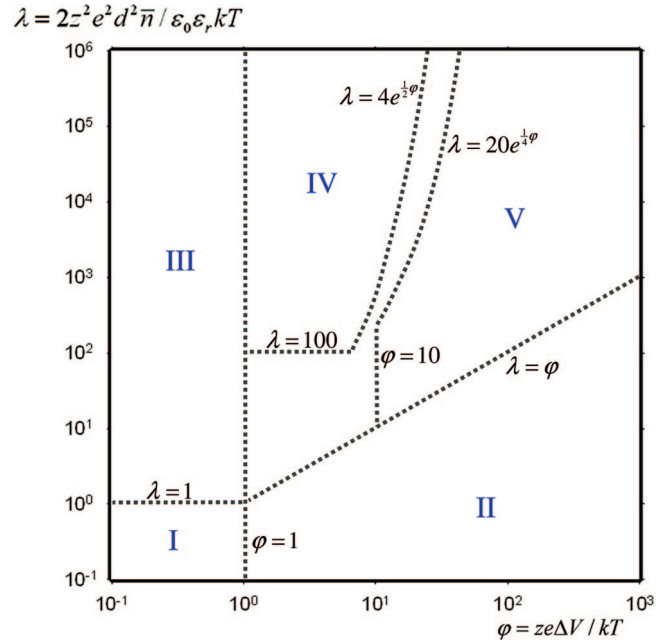

Figure 2. Overview of five analytical regimes in φ, λ parameter space.

1.2. Gouy−Chapman Solution. The Gouy−Chapman (GC) solution is derived in numerous leading textbooks[18–22] as a solution of the planar PB eq 8. However, the GC solution is not its general solution, since it makes a further assumption! In all mentioned textbooks, it is derived for the case of a single isolated charged plate immersed in electrolyte. Here, we reproduce the derivation but for the extended case of two oppositely charged plates. Following the classical analysis of Gouy[16] and Chapman,[17] eq 8 is multiplied by $2\partial\tilde{V}/\partial\tilde{x}$ on both sides and integrated over $\tilde{x}$

$$\int \frac{\partial}{\partial \tilde{x}}\left(\frac{\partial \tilde{V}}{\partial \tilde{x}}\right)^2 d\tilde{x} = \int 2\lambda_0 \sinh(\tilde{V}) d\tilde{V} \tag{9}$$

If the integration is performed starting from the midplane $\tilde{x} = 0$ where $\tilde{V} = 0$, it follows that

$$\left(\frac{\partial \tilde{V}}{\partial \tilde{x}}\right)^2 = \left(\frac{\partial \tilde{V}}{\partial \tilde{x}}\right)^2_{\tilde{x}=0} + 2\lambda_0[\cosh(\tilde{V}) - 1] \tag{10}$$

Now, the further assumption of the GC approach is that there exists a region where the electric field is negligibly small. For the special case of two identically charged plates, this assumption is fully justified since the midplane by symmetry combines zero potential and zero field. However, in all other cases, this implies the presence of a "bulk electrolyte" region. From the Boltzmann eq 4, it follows that uniform potential (zero field) implies uniform concentration of all ionic species ("bulk"). Under electroneutrality conditions, this "bulk" region forms a trivial solution of the PB eq 6. For a single charged plate, it makes sense to assume "bulk electrolyte" at infinity. However, for the present case of two oppositely charged plates, we cannot a priori justify this assumption (which is also recognized elsewhere[28]). Nevertheless, if we make the GC assumption $\partial\tilde{V}/\partial\tilde{x}|_{\tilde{x}=0} = 0$, then it follows that

$$\frac{\partial \tilde{V}}{\partial \tilde{x}} = -\sqrt{4\lambda_0}\left|\sinh\left(\frac{1}{2}\tilde{V}\right)\right| \quad (11)$$

Solving this from the lower boundary $\tilde{x} = -1/2$ where $\tilde{V} = {}^1/_2\varphi$ gives

$$\tilde{V} = 2\ln\left[\frac{1+\tanh\left(\frac{1}{8}\varphi\right)\exp\left(-\sqrt{\lambda_0}\left(\frac{1}{2}+\tilde{x}\right)\right)}{1-\tanh\left(\frac{1}{8}\varphi\right)\exp\left(-\sqrt{\lambda_0}\left(\frac{1}{2}+\tilde{x}\right)\right)}\right] \quad -\frac{1}{2} \le \tilde{x} < 0$$

$$\tilde{V} = 2\ln\left[\frac{1-\tanh\left(\frac{1}{8}\varphi\right)\exp\left(-\sqrt{\lambda_0}\left(\frac{1}{2}-\tilde{x}\right)\right)}{1+\tanh\left(\frac{1}{8}\varphi\right)\exp\left(-\sqrt{\lambda_0}\left(\frac{1}{2}-\tilde{x}\right)\right)}\right] \quad 0 < \tilde{x} \le \frac{1}{2} \quad (12)$$

This eq 12 is referred to as the GC solution, describing the potential profile as a function of the dimensionless midplane concentration λ_0 and electrode potential difference φ. This GC solution is widely used, often to successfully explain measurement results.

Now we investigate a posteriori the reasonability of the "zero field" assumption, by calculating the first order estimates of $\tilde{V}$ and $\partial\tilde{V}/\partial\tilde{x}$ at the midplane $\tilde{x} = 0$ with eq 12 and eq 11:

$$\tilde{V}\Big|_{\tilde{x}=0} \approx 4\tanh\left(\frac{1}{8}\varphi\right)\exp\left(-\frac{1}{2}\sqrt{\lambda_0}\right) \quad (13)$$

$$-\frac{\partial \tilde{V}}{\partial \tilde{x}}\Big|_{\tilde{x}=0} \approx \sqrt{4\lambda_0}\,2\tanh\left(\frac{1}{8}\varphi\right)\exp\left(-\frac{1}{2}\sqrt{\lambda_0}\right) \quad (14)$$

In recalling both assumptions, the midplane potential estimate $\tilde{V}|_{\tilde{x}=0}$ should be much lower than the maximum potential ${}^1/_2\varphi$ and the midplane field estimate $(-\partial\tilde{V}/\partial\tilde{x})|_{\tilde{x}=0}$ should be much lower than the average electric field $\langle -\partial\tilde{V}/\partial\tilde{x}\rangle = \varphi$. Both conditions are only fulfilled with a minimum midplane concentration $\lambda_0 > 100$, in which case the midplane electric field becomes less than 3% of the average field.

This minimum midplane concentration $\lambda_0 > 100$ can be converted into a minimum required average ion concentration. The net charge Q_{net} inside an electric double layer is calculated with Gauss' law applied over the half-space between $\tilde{x} = -1/2$ and $\tilde{x} = 0$, and eq 11

$$Q_{net} = \frac{kT}{zed}\left(\frac{\partial\tilde{V}}{\partial\tilde{x}}\Big|_{\tilde{x}=-1/2} - \frac{\partial\tilde{V}}{\partial\tilde{x}}\Big|_{\tilde{x}=0}\right)\varepsilon_0\varepsilon_r A = 2\sqrt{\lambda_0}\sinh\left(\frac{1}{4}\varphi\right)\frac{\varepsilon_0\varepsilon_r kT}{zed}A \quad (15)$$

Here, A denotes the area of the parallel plate device (in m^2). Q_{net} is the result of separation of the positive and negative ions, and therefore can never exceed the total positive ionic charge (in the whole space) $Q_{total} = ze\bar{n}dA$. The requirement $Q_{total} \ge Q_{net}$ imposes a minimum value on the average ion concentration

$$\bar{n} > 2\sqrt{\lambda_0}\sinh\left(\frac{ze\Delta V}{4kT}\right)\frac{\varepsilon_0\varepsilon_r kT}{z^2e^2d^2} > 20\sinh\left(\frac{ze\Delta V}{4kT}\right)\frac{\varepsilon_0\varepsilon_r kT}{z^2e^2d^2} \quad (16)$$

For a 1 cm thick device with univalent ions in water at 2 V potential difference, the average ion concentration should therefore exceed $10^{20}\ m^{-3} \cong 0.2\ \mu M$. This demonstrates that in conventional electrochemical experiments the GC solution may indeed be applicable. However, for a microdevice ($d = 10\ \mu m$) with the same univalent ions and 2 V potential difference, the GC validity requires an ion concentration above 0.2 M: a severe restriction. Moreover, for many applications in nonaqueous microdevices, 5 V is realistic. In that case, the exponential voltage dependence of the above condition eq 16 would require unrealistically high concentrations (10^{11}M!) in order for the GC solution to hold.

We conclude that the "zero field" assumption of the GC solution may be reasonable for macroscopic containers, but for microdevices, it is a limiting assumption!

2. Complete Solution

To extend the range of validity, we now return to the Poisson−Boltzmann equation and solve it without assuming the presence of a "bulk electrolyte" region with zero field. We again consider a symmetrical z:z electrolyte: $z^+ = -z^- = z$. Charge neutrality over the device as a whole dictates $\int_{-d/2}^{d/2} n^+ dx = \int_{-d/2}^{d/2} n^- dx = \bar{n}d$. A total potential difference ΔV is applied between both electrodes (separated by a distance d), and therefore the integrated electric field should be equal to $\int_{-d/2}^{d/2} E dx = \Delta V$. These quantities can be used for defining the following dimensionless variables

$$\tilde{x} \equiv \frac{x}{d} \quad \tilde{n}^{\pm} \equiv \frac{n^{\pm}d}{\int n^{\pm}dx} = \frac{n^{\pm}}{\bar{n}} \quad \tilde{E} \equiv \frac{Ed}{\int E dx} = \frac{Ed}{\Delta V} \quad (17)$$

Dimensionless parameters related to the applied voltage and average concentration are defined similar to elsewhere[29] as

$$\varphi \equiv \frac{ze\Delta V}{kT} \quad \text{and} \quad \lambda \equiv \frac{2\bar{n}z^2e^2d^2}{\varepsilon_0\varepsilon_r kT} \quad (18)$$

Then eq 3 and eq 5 can be rewritten as

$$\varphi\tilde{n}^{\pm}\tilde{E} = \pm\frac{\partial\tilde{n}^{\pm}}{\partial\tilde{x}} \quad (19)$$

$$\varphi\frac{\partial\tilde{E}}{\partial\tilde{x}} = \frac{1}{2}\lambda(\tilde{n}^+ - \tilde{n}^-) \quad (20)$$

The solution of eq 19 and eq 20 is fully equivalent to the Poisson−Boltzmann formulation of eq 8, but, as will become clear later, it is beneficial to use λ (average concentration) as a parameter instead of λ_0 (midplane concentration). The solution applies both to strong and to weak electrolytes, as long as the average number of ions (and therefore the average concentration $\bar{n}$) is known in the steady-state situation.

The concentration profiles of positive and negative ions are each other's mirror image over the midplane $\tilde{x} = 0$. This can be seen from the above equations, as interchanging both electrodes by reversing the voltage φ mathematically has the same effect as interchanging positive $\tilde{n}^+$ and negative $\tilde{n}^-$ concentrations. As a consequence, the midplane concentrations are equal: $\tilde{n}_0^+ = \tilde{n}_0^- = \tilde{n}_0$. Second, the electric field $\tilde{E}$ will be symmetrical around the midplane. As a third consequence, both concentration profiles $\tilde{n}^+$ and $\tilde{n}^-$ will be monotonous functions.

The concentration and field profiles that follow from solving eq 19 and eq 20 will depend strongly on the values of parameters φ and λ. In this paper, the major part of the φ,λ parameter space is subdivided into five regimes I−V as indicated in Figure 2. In the following five sections, each regime will be discussed separately by deriving analytical approximations for the corresponding concentration and field profiles. The approach will be to make "ansatz" assumptions on the concentration and field profiles, derive the full profiles, and afterward inspect their region of validity in terms of φ and λ.

2.1. Limiting Case I: Uniform *n*,*E*. In this simplest limiting case, we assume that both the concentration and the electric field profiles are uniform to first order: $\tilde{n}^{\pm} = 1 + f(\tilde{x})$ and $\tilde{E} = 1 + g(\tilde{x})$ with $|f(\tilde{x})| \ll 1$ and $|g(\tilde{x})| \ll 1$. Under that assumption,

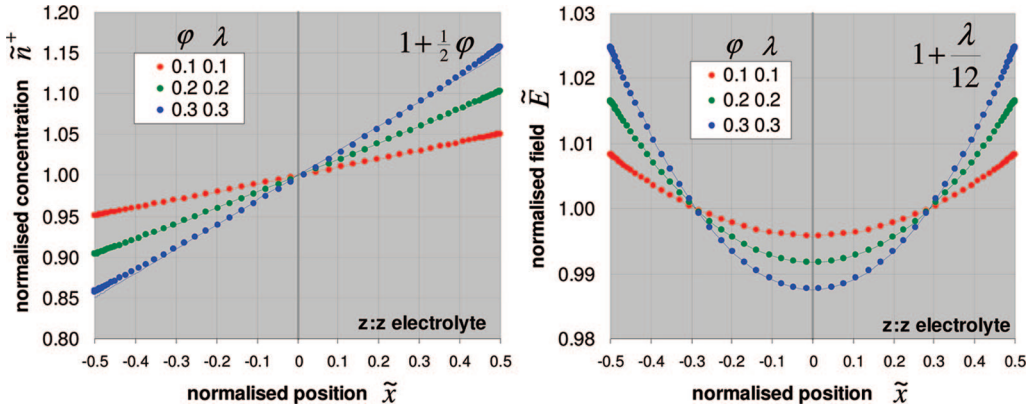

Figure 3. Concentration and field profiles for limiting case I of uniform n,E in the range φ, $\lambda < 1$. Symbols denote the numerical solution; lines denote the analytical approximations.

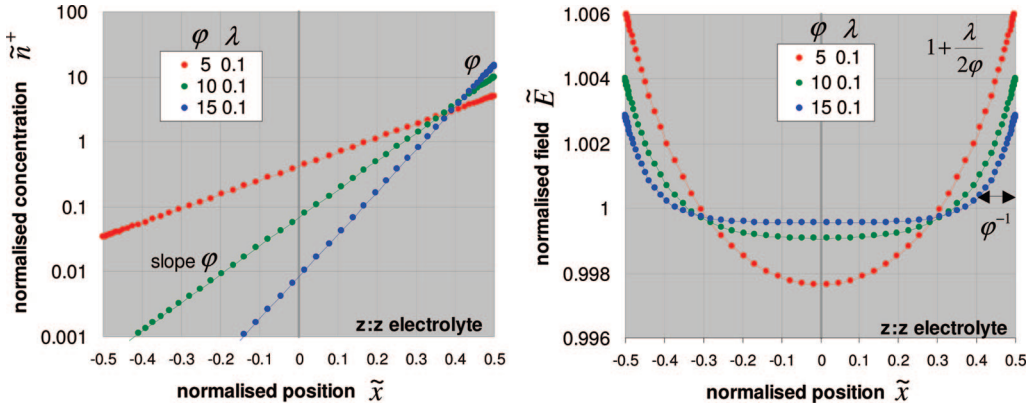

Figure 4. Concentration and field profiles for limiting case II of uniform E in the range $\lambda < \varphi$ and $\varphi > 1$. Symbols denote the numerical solution; lines denote the analytical approximations.

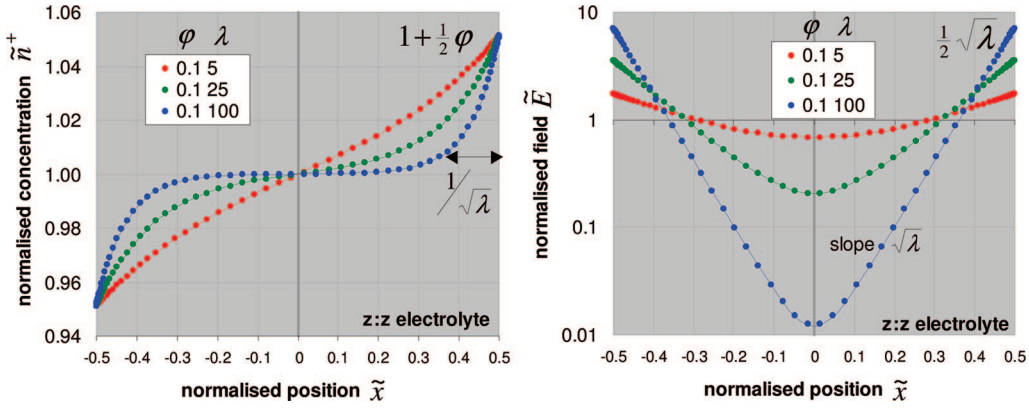

Figure 5. Concentration and field profiles for limiting case III of uniform n in the range $\varphi < 1$ and $\lambda > 1$. Symbols denote the numerical solution; lines denote the analytical approximations.

we can calculate $\tilde{n}^{\pm}$ by approximating $\tilde{E} \approx 1$ in eq 19, integrating and using the first order Taylor approximation

$$\tilde{n}^{\pm} \approx \tilde{n}_0^{\pm} \exp(\pm\varphi\tilde{x}) \approx 1 \pm \varphi\tilde{x} \tag{21}$$

Then, by integrating eq 20 and normalizing, we can calculate $\tilde{E}$

$$\tilde{E} \approx \tilde{E}_0 + \frac{1}{2}\lambda\tilde{x}^2 = 1 + \frac{1}{2}\lambda\left(\tilde{x}^2 - \frac{1}{12}\right) \tag{22}$$

The range of validity of expressions 21 and 22 is obtained by self-consistently returning to our assumptions. In order for the $\tilde{n}^{\pm}$ profile to be uniform (within 50%), the condition $\varphi < 1$ should hold, and similarly $\lambda < 1$ for a uniform $\tilde{E}$ profile (within 10%).

In Figure 3, concentration and field profiles are depicted for three sets of φ,λ parameter values within the obtained range of validity. Only the concentration profile of positive ions $\tilde{n}^+$ is plotted here and in all further graphs, since the negative profile $\tilde{n}^-$ is always identical, but mirrored over the midplane $\tilde{x} = 0$. The drawn curves are calculated with expressions 21 and 22. Also indicated are dots that represent the results of the complete numerical solution (that will be

discussed in a later section). The agreement with the numerical results demonstrates their validity within the range $\varphi,\lambda < 1$. Also indicated are the expressions for easy calculation of concentration $\tilde{n}^{+}_{1/2} = 1 + {}^1/_2\varphi$ and field $\tilde{E}_{1/2} = 1 + {}^1/_{12}\lambda$ at the upper electrode. For a more accurate estimation of the midplane concentration, we can refine the above calculation based on the second order expansion of concentration $\tilde{n}^{\pm}$, to obtain: $\tilde{n}_0 = 1 - {}^1/_{24}\varphi^2$.

2.2. Limiting Case II: Uniform *E*. In the limiting case that we assume only the electric field profile to be uniform to first order $\tilde{E} = 1 + g(\tilde{x})$, we can again obtain $\tilde{n}^{\pm}$ by approximating $\tilde{E} \approx 1$ in eq 19, integrating, and subsequently normalizing.

$$\tilde{n}^{\pm} \approx \tilde{n}^{\pm}_0 \exp(\pm\varphi\tilde{x}) = \frac{\frac{1}{2}\varphi}{\sinh\left(\frac{1}{2}\varphi\right)} \exp(\pm\varphi\tilde{x}) \qquad (23)$$

Substituting this solution into eq 20, integrating, and normalizing gives

$$\tilde{E} \approx \frac{\lambda}{2\varphi}\frac{\cosh(\varphi\tilde{x}) - 1}{\sinh\left(\frac{1}{2}\varphi\right)} + \tilde{E}_0 = 1 + \frac{\lambda}{\varphi}\left(\frac{\cosh(\varphi\tilde{x})}{2\sinh\left(\frac{1}{2}\varphi\right)} - \frac{1}{\varphi}\right) \qquad (24)$$

The concentration and field profiles are plotted in Figure 4. The obtained electric field (eq 24) is uniform (within 50%) as assumed, under the condition $\lambda < \varphi$. In the limit of small $\varphi \ll 1$, expressions 23 and 24 indeed become identical to the "uniform *n*,*E*" expressions 21 and 22. In the limit of high $\varphi \gg 1$, the concentration and field at the electrodes become $\tilde{n}^{+}_{1/2} = \varphi$, $\tilde{n}^{+}_{-1/2} = \varphi/\exp(\varphi)$, and $\tilde{E}_{\pm 1/2} = 1 + \lambda/2\varphi$, at the midplane $\tilde{n}_0 = {}^1/_2\varphi/\sinh({}^1/_2\varphi)$ and $\tilde{E}_0 = 1 - \lambda/\varphi^2$.

2.3. Limiting Case III: Uniform *n*. In this limiting case, we assume that only the concentration profile is uniform to first order $\tilde{n}^{\pm} = 1 + f(\tilde{x})$. If we take the derivative of eq 20, substitute eq 19, and use the assumption $\tilde{n}^{\pm} \approx 1$, we obtain

$$\varphi\frac{\partial^2\tilde{E}}{\partial\tilde{x}^2} = \frac{1}{2}\lambda\left(\frac{\partial\tilde{n}^{+}}{\partial\tilde{x}} - \frac{\partial\tilde{n}^{-}}{\partial\tilde{x}}\right) = \frac{1}{2}\lambda\varphi\tilde{E}(\tilde{n}^{+} + \tilde{n}^{-}) \approx \lambda\varphi\tilde{E} \qquad (25)$$

Integrating and normalizing gives

$$\tilde{E} = \tilde{E}_0\cosh(\sqrt{\lambda}\tilde{x}) = \frac{\frac{1}{2}\sqrt{\lambda}}{\sinh\left(\frac{1}{2}\sqrt{\lambda}\right)}\cosh(\sqrt{\lambda}\tilde{x}) \qquad (26)$$

Subsequently, $\tilde{n}^{\pm}$ can be determined with eq 19 as

$$\frac{1}{\tilde{n}^{\pm}}\frac{\partial\tilde{n}^{\pm}}{\partial\tilde{x}} = \pm\varphi\tilde{E} = \pm\varphi\frac{\frac{1}{2}\sqrt{\lambda}}{\sinh\left(\frac{1}{2}\sqrt{\lambda}\right)}\cosh(\sqrt{\lambda}\tilde{x}) \qquad (27)$$

Integrating, taking the first order Taylor expansion (as assumed $\tilde{n}^{\pm} \approx 1$) and normalizing gives

$$\tilde{n}^{\pm} = \tilde{n}_0\exp\left(\pm\frac{\frac{1}{2}\varphi}{\sinh\left(\frac{1}{2}\sqrt{\lambda}\right)}\sinh(\sqrt{\lambda}\tilde{x})\right) \approx 1 \pm \frac{1}{2}\varphi\frac{\sinh(\sqrt{\lambda}\tilde{x})}{\sinh\left(\frac{1}{2}\sqrt{\lambda}\right)} \qquad (28)$$

The obtained concentration profile (eq 28) is uniform (within 50%) in the range $\varphi < 1$. This condition of small voltage $\varphi < 1$ is also the basis of the well-known Debye−Hückel[15] linearization of the Poisson−Boltzmann equation. In that approximate solution, exactly as in eq 26, the electric field decays exponentially away from the electrodes (as in Figure 5). Now it becomes clear that our dimensionless concentration parameter $\lambda \equiv (2z^2e^2d^2\bar{n})/(\varepsilon_0\varepsilon_r kT)$ is closely related to the well-known Debye−Hückel parameter $\kappa \equiv \sqrt{e^2\sum_i n_0^i(z^i)^2/(\varepsilon_0\varepsilon_r kT)}$. For a symmetrical z:z electrolyte, $\lambda_0 \equiv \kappa^2d^2$. The advantage of parameter λ instead of the usual κ will become apparent in a later section (on the "separated *n*" regime).

In the limit of small $\lambda \ll 1$, the concentration (eq 28) and field (eq 26) profiles again become equal to expressions 21 and 22 of the uniform *n*,*E* limiting case. In the limit of high $\lambda \gg 1$, the electric field at the electrodes becomes $\tilde{E}_{\pm 1}/_2 = {}^1/_2\sqrt{\lambda}$, and at the midplane $\tilde{E}_0 = ({}^1/_2\sqrt{\lambda})/\sinh({}^1/_2\sqrt{\lambda})$. For a more accurate estimation of the midplane concentration, we add the second order Taylor term to concentration profile (eq 28), and normalization gives $\tilde{n}_0 = 1 - {}^1/_8\varphi^2[1 - \sinh(\sqrt{\lambda})/\sqrt{\lambda}]/[1 - \cosh(\sqrt{\lambda})]$.

2.4. Limiting Case IV: Screened *E*. In this limiting case, we make two assumptions about the field and concentration at the midplane ($\tilde{x} = 0$): $\tilde{E}_0 \ll 1$ and $\tilde{n}_0 \approx 1$.

The second assumption means that the midplane concentration n_0 is equal to the average concentration $\bar{n}$. This is equivalent to assuming that λ_0 and λ are equal:

$$\lambda_0 \equiv \frac{2n_0z^2e^2d^2}{\varepsilon_0\varepsilon_r kT} = \frac{2z^2e^2d^2}{\varepsilon_0\varepsilon_r kT}\tilde{n}_0\bar{n} = \tilde{n}_0\lambda \approx \lambda \qquad (29)$$

The first assumption $\tilde{E}_0 \ll 1$ is identical to the (tacit) assumption of Gouy−Chapman. Therefore, the solutions can be derived from equation 12 by substituting $\lambda_0 \approx \lambda$.

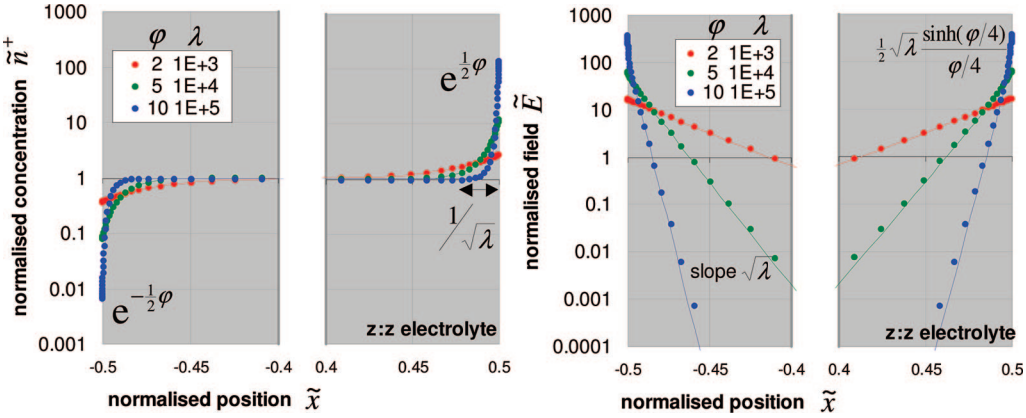

Figure 6. Concentration and field profiles for limiting case IV of screened *E* in the range $\lambda > 100$ and $\lambda > 4\exp({}^1/_2\varphi)$. Symbols denote the numerical solution; lines denote the analytical approximations.

$$\tilde{V} = 2\ln\left[\frac{1+\tanh\left(\frac{1}{8}\varphi\right)\exp\left(-\sqrt{\lambda}\left(\frac{1}{2}+\tilde{x}\right)\right)}{1-\tanh\left(\frac{1}{8}\varphi\right)\exp\left(-\sqrt{\lambda}\left(\frac{1}{2}+\tilde{x}\right)\right)}\right] \quad -\frac{1}{2}\le\tilde{x}<0$$

$$\tilde{V} = 2\ln\left[\frac{1-\tanh\left(\frac{1}{8}\varphi\right)\exp\left(-\sqrt{\lambda}\left(\frac{1}{2}-\tilde{x}\right)\right)}{1+\tanh\left(\frac{1}{8}\varphi\right)\exp\left(-\sqrt{\lambda}\left(\frac{1}{2}-\tilde{x}\right)\right)}\right] \quad 0<\tilde{x}\le\frac{1}{2} \quad (30)$$

The normalized electric field profile $\tilde{E}$ can be calculated from $\tilde{V}$ by taking the derivative $\tilde{E} \equiv Ed/\Delta V = -\partial V/\partial x \cdot d/\Delta V = -\partial\tilde{V}/\partial\tilde{x}\cdot kT/ze\Delta V = -\partial\tilde{V}/\partial\tilde{x}\cdot 1/\varphi$.

$$\tilde{E} = \frac{4\sqrt{\lambda}\tanh\left(\frac{1}{8}\varphi\right)\exp\left(-\sqrt{\lambda}\left(\frac{1}{2}+\tilde{x}\right)\right)}{\varphi-\varphi\tanh^2\left(\frac{1}{8}\varphi\right)\exp\left(-2\sqrt{\lambda}\left(\frac{1}{2}+\tilde{x}\right)\right)} \quad -\frac{1}{2}\le\tilde{x}<0$$

$$\tilde{E} = \frac{4\sqrt{\lambda}\tanh\left(\frac{1}{8}\varphi\right)\exp\left(-\sqrt{\lambda}\left(\frac{1}{2}-\tilde{x}\right)\right)}{\varphi-\varphi\tanh^2\left(\frac{1}{8}\varphi\right)\exp\left(-2\sqrt{\lambda}\left(\frac{1}{2}-\tilde{x}\right)\right)} \quad 0<\tilde{x}\le\frac{1}{2} \quad (31)$$

Also, the normalized concentration profiles $\tilde{n}^{\pm}$ follow from $\tilde{V}$. With eq 4, $\tilde{n}^{\pm} = (n_0/\bar{n})\exp(-z^{\pm}eV/kT) = \tilde{n}_0\exp(\mp\tilde{V})$ and assuming midplane concentration $\tilde{n}_0 \approx 1$, it follows

$$\tilde{n}^{\pm} = \left[\frac{1-\tanh\left(\frac{1}{8}\varphi\right)\exp\left(-\sqrt{\lambda}\left(\frac{1}{2}+\tilde{x}\right)\right)}{1+\tanh\left(\frac{1}{8}\varphi\right)\exp\left(-\sqrt{\lambda}\left(\frac{1}{2}+\tilde{x}\right)\right)}\right]^{\pm 2} \quad -\frac{1}{2}\le\tilde{x}<0$$

$$\tilde{n}^{\pm} = \left[\frac{1+\tanh\left(\frac{1}{8}\varphi\right)\exp\left(-\sqrt{\lambda}\left(\frac{1}{2}-\tilde{x}\right)\right)}{1-\tanh\left(\frac{1}{8}\varphi\right)\exp\left(-\sqrt{\lambda}\left(\frac{1}{2}-\tilde{x}\right)\right)}\right]^{\pm 2} \quad 0<\tilde{x}\le\frac{1}{2} \quad (32)$$

The obtained expressions for field (eq 31) and concentration (eq 32) are plotted in Figure 6. The applicability range of the Gouy−Chapman solution was established in equations 13, 14, and 16: $\lambda_0 > 100$ and $^1/_2\lambda > 2\sqrt{\lambda_0}\sinh(^1/_4\varphi)$. Therefore, the range where $\tilde{E}_0 \ll 1$ becomes $\lambda > 20\exp(^1/_4\varphi)$. With the additional assumption that $\lambda_0 \approx \lambda$, the range where also $\tilde{n}_0 \approx 1$ becomes: $\lambda > 100$ and $\lambda > 4\exp(^1/_2\varphi)$.

The actual midplane concentration $\tilde{n}_0$ can be obtained by normalization of the concentration profile (eq 32) to obtain: $\tilde{n}_0 = [1 + \{\cosh(^1/_4\varphi) - 1\}/^1/_4\sqrt{\lambda}]^{-1}$. For the above determined φ,λ range, indeed we find that the assumption $\tilde{n}_0 \approx 1$ holds. In this same range, the normalization integral of the field profile is also equal to unity.

At the electrodes, the field (eq 31) and concentration (eq 32) reduce to $\tilde{E}_{\pm 1/2} = ^1/_2\sqrt{\lambda}\,[\sinh(\varphi/4)]/(\varphi/4)$ and $\tilde{n}^{+}_{\pm 1/2} = \exp(\pm^1/_2\varphi)$. In the limit of small $\varphi \ll 1$, field (eq 31) and concentration (eq 32) profiles indeed become equal to those of the "uniform n" limiting case, being expressions 26 and 28 for $\lambda > 100$ and $\tilde{x} \neq 0$. At the midplane $\tilde{x} = 0$, the obtained potential (eq 30) for this limiting case has a discontinuity. Around the midplane, the potential is best approximated by the sum of both half-space potential profiles $\tilde{V} \approx -8\tanh(^1/_8\varphi)\exp(-^1/_2\sqrt{\lambda})\sinh(\sqrt{\lambda}\tilde{x})$. With that, the midplane field becomes $\tilde{E}_0 \equiv -(1/\varphi)\cdot(\partial\tilde{V}/\partial\tilde{x})|_{\tilde{x}=0} = [(\tanh(^1/_8\varphi))/(^1/_8\varphi)][\sqrt{\lambda}/\exp(^1/_2\sqrt{\lambda})]$.

2.5. Limiting Case V: Separated *n*. In this final limiting case, we make the following two assumptions about the field and concentration at the midplane ($\tilde{x} = 0$): $\tilde{E}_0 \approx 1$ and $\tilde{n}_0 \ll 1$. Notice that mathematically this is complementary to "screened E". Since the concentration profiles have to be monotonous functions, the second assumption implies that all ions are separated: the positive ions are located in the positive half-space $\tilde{x} > 0$, and all negative ions in the negative half-space $\tilde{x} < 0$.

Multiplying eq 20 on both sides with $\varphi\tilde{E}$ and substituting eq 19 gives

$$\varphi^2\tilde{E}\frac{\partial\tilde{E}}{\partial\tilde{x}} = \frac{1}{2}\lambda(\tilde{n}^{+}-\tilde{n}^{-})\varphi\tilde{E} = \frac{1}{2}\lambda\left(\frac{\partial\tilde{n}^{+}}{\partial\tilde{x}}+\frac{\partial\tilde{n}^{-}}{\partial\tilde{x}}\right) \quad (33)$$

Integrating this equation yields that $^1/_2\varphi^2\,\tilde{E}^2 - ^1/_2\lambda(\tilde{n}^{+}+\tilde{n}^{-})$ is independent of $\tilde{x}$ (uniform). With the above assumptions at the midplane, it follows that

$$\frac{1}{2}\varphi^2\tilde{E}^2 - \frac{1}{2}\lambda(\tilde{n}^{+}+\tilde{n}^{-}) = \frac{1}{2}\varphi^2 \quad (34)$$

In the positive half-space ($\tilde{x} > 0$), the positive species dominate the negative: $\tilde{n}^{+} \gg \tilde{n}^{-}$. Then eq 20 and eq 34 can be combined into

$$\varphi\frac{\partial\tilde{E}}{\partial\tilde{x}} = \frac{1}{2}\lambda\tilde{n}^{+} = \frac{1}{2}\varphi^2(\tilde{E}^2-1) \quad (35)$$

For the region where $\tilde{E} > 1$, eq 35 has the following solution

$$\tilde{E} = \frac{1}{\tanh\left[\frac{1}{2}\varphi\left(\frac{1}{2}-\tilde{x}\right)+\operatorname{arctanh}\left(\frac{2\varphi}{2\varphi+\lambda}\right)\right]} \quad 0<\tilde{x}\le\frac{1}{2} \quad (36)$$

Here the upper boundary condition for the field $\tilde{E}_{1/2}$ at the electrode is used, which can be found by integrating eq 20 in the positive half-space, using the assumption that all positive charge $\tilde{n}^{+}$ is separated into the positive half-space.

$$\tilde{E}_{1/2} = \tilde{E}_0 + \int_0^{1/2}\frac{\partial\tilde{E}}{\partial\tilde{x}}d\tilde{x} \approx 1 + \frac{\lambda}{2\varphi}\int_0^{1/2}(\tilde{n}^{+}-\tilde{n}^{-})d\tilde{x} \approx 1 + \frac{\lambda}{2\varphi}\int_0^{1/2}\tilde{n}^{+}d\tilde{x} \approx 1 + \frac{\lambda}{2\varphi} \quad (37)$$

The concentration profile follows from eq 35 by taking the derivative of the field profile (eq 36) as

$$\tilde{n}^{+} = \frac{\varphi^2}{\lambda}\frac{1}{\sinh^2\left[\frac{1}{2}\varphi\left(\frac{1}{2}-\tilde{x}\right)+\operatorname{arctanh}\left(\frac{2\varphi}{2\varphi+\lambda}\right)\right]} \quad 0<\tilde{x}\le\frac{1}{2} \quad (38)$$

At the upper electrode, this expression (eq 38) reduces to $\tilde{n}^{+}_{1/2} = \varphi + ^1/_4\lambda$.

From symmetry considerations, also the solutions in the negative half-space are known:

$$\tilde{E} = \frac{1}{\tanh\left[\frac{1}{2}\varphi\left(\frac{1}{2}+\tilde{x}\right)+\operatorname{arctanh}\left(\frac{2\varphi}{2\varphi+\lambda}\right)\right]} \quad -\frac{1}{2}\le\tilde{x}<0$$

$$\tilde{n}^{-} = \frac{\varphi^2}{\lambda}\frac{1}{\sinh^2\left[\frac{1}{2}\varphi\left(\frac{1}{2}+\tilde{x}\right)+\operatorname{arctanh}\left(\frac{2\varphi}{2\varphi+\lambda}\right)\right]} \quad -\frac{1}{2}\le\tilde{x}<0 \quad (39)$$

In Figure 7 the obtained concentration and field profiles are depicted.

The validity range of expressions 36, 38, and 39 over the φ,λ space is obtained from re-evaluating the assumptions with the obtained profiles. The assumed separation of ions implies that $\tilde{n}^{+}_0 \ll \tilde{n}^{+}_{1/2}$, and therefore with eq 38, $^1/_4\varphi \gg \operatorname{arctanh}[2\varphi/(2\varphi+\lambda)]$. The first assumption ($\tilde{E}_0 \approx 1$) with eq 36 then becomes $\tilde{E}_0 = 1/\tanh[^1/_4\varphi] \approx 1$, which is satisfied for $\varphi > 10$. Away from the upper electrode, expression 38 can be ap-

proximated as $\tilde{n}^+ = [\varphi^2/(\varphi + {}^1/_4\lambda)]\exp(\varphi\tilde{x})/\exp({}^1/_2\varphi)$, using the identity $\operatorname{arctanh}(x) = {}^1/_2\ln[(1+x)/(1-x)]$. The concentrations at the midplane and left electrode then become $\tilde{n}_0^+ = [\varphi/(\varphi + {}^1/_4\lambda)]\cdot\varphi/\exp({}^1/_2\varphi)$ and $\tilde{n}_{-1/2}^{\pm} = [\varphi/(\varphi + {}^1/_4\lambda)]\cdot\varphi/\exp(\varphi)$.

A second assumption is that, in the derivation of eq 36, we have used a boundary condition at the upper electrode, but of course also the field normalization condition (eq 17) should hold:

$$\int_0^{1/2}(\tilde{E}-1)d\tilde{x} = -\frac{1}{2} - \frac{2}{\varphi}\ln\left(\frac{2\varphi}{\sqrt{\lambda(\lambda+4\varphi)}}\right) + \frac{2}{\varphi}\ln\left(\sinh\left[\frac{1}{4}\varphi + \operatorname{arctanh}\left(\frac{2\varphi}{\lambda+2\varphi}\right)\right]\right) \approx \frac{2}{\varphi}\ln\left(\frac{\lambda+4\varphi}{4\varphi}\right) \ll 1$$

This is fulfilled for $\lambda < 20\exp({}^1/_4\varphi)$, so just outside the region in the φ,λ space where the midplane field becomes zero (as derived in the previous section). The normalization condition above can be used to calculate a more accurate estimate of the midplane field $\tilde{E}_0 = 1 - (4/\varphi)\ln[(\lambda+4\varphi)/4\varphi]$.

In the limit of $\lambda < \varphi$, the concentration profile (eq 38) becomes equal to expression 23 of the "uniform E" limiting case (with $\varphi > 10$, and again using the arctanh identity).

In this "separated n" regime, we can appreciate the benefit of using λ as a parameter instead of λ_0 or κ, because the latter two are based on the midplane concentration which becomes negligibly small (at high voltages). In addition, the usual physical interpretation of κ^{-1} as the characteristic double layer thickness is no longer valid, but instead φ^{-1} is a more appropriate characteristic in this regime.

2.6. Numerical Solution. In this paragraph, the complete numerical solution of the planar Poisson−Boltzmann equation will be given. This numerical solution is in full agreement with the analytical (approximate) solutions derived in the previous paragraphs for the five limiting cases, as shown in Figure 3 through Figure 7.

The numerical solution is determined by the set of equations 19 and 20 and normalization conditions:

$$\varphi\tilde{n}^{\pm}\tilde{E} = \pm\frac{\partial\tilde{n}^{\pm}}{\partial\tilde{x}} \quad \varphi\frac{\partial\tilde{E}}{\partial\tilde{x}} = \frac{1}{2}\lambda(\tilde{n}^+ - \tilde{n}^-)$$
$$\int_{-1/2}^{1/2}\tilde{n}^{\pm}d\tilde{x} = 1 \quad \int_{-1/2}^{1/2}\tilde{E}d\tilde{x} = 1 \qquad (40)$$

Numerically this first set of equations is impractical to solve as it does not comply with the usual scheme of differential equations with known boundary conditions. Therefore, we introduce a second set of time-dependent partial differential equations (with normalized time parameter $\tilde{t}$), boundary conditions (bc) and intitial conditions (ic). Mathematically the steady-state solution of this second set is equal to the solution of the first set. The physical origin of this time-dependence is the continuity equation applied to the Nernst−Planck transport equation.

$$\frac{d\tilde{n}^{\pm}}{d\tilde{t}} = \frac{\partial}{\partial\tilde{x}}\left(\pm\tilde{n}^{\pm}\frac{\partial\tilde{V}}{\partial\tilde{x}} + \frac{\partial\tilde{n}^{\pm}}{\partial\tilde{x}}\right) \qquad (41)$$

$$\frac{\partial^2\tilde{V}}{\partial\tilde{x}^2} = -\frac{1}{2}\lambda(\tilde{n}^+ - \tilde{n}^-) \qquad (42)$$

$$\text{bc:} \quad \left(\pm\tilde{n}^{\pm}\frac{\partial\tilde{V}}{\partial\tilde{x}} + \frac{\partial\tilde{n}^{\pm}}{\partial\tilde{x}}\right)_{\tilde{x}=\pm 1/2} = 0 \quad \tilde{V}_{\pm 1/2} = \mp\frac{1}{2}\varphi\frac{\tilde{t}}{1+\tilde{t}} \qquad (43)$$

$$\text{ic}(\tilde{t}=0): \qquad \tilde{n}^{\pm} = 1 \quad \tilde{V} = 0 \qquad (44)$$

Here, the normalized voltage is introduced again as $\tilde{V} \equiv zeV/kT$. Therefore, the identity $\tilde{E} = -(1/\varphi)(\partial\tilde{V}/\partial\tilde{x})$ holds, and eq 42 immediately becomes identical to the second equation of the first set (eq 40). The steady-state solution of eq 41 in combination with the boundary condition (eq 43) reduces to the first equation of the first set. Integration of eq 41 over the entire space between $\tilde{x} = \pm 1/2$ in combination with the boundary condition (eq 43) gives $d(\int_{-1/2}^{1/2}\tilde{n}^{\pm}d\tilde{x})/d\tilde{t} = 0$. With the initial condition (eq 44) the concentration normalization (third equation) of the first set $\int_{-1/2}^{1/2}\tilde{n}^{\pm}\,d\tilde{x} = 1$ is retrieved. Finally, the field normalization (fourth equation of first set) is obtained in the steady-state $\tilde{t}\to\infty$ from the boundary conditions (eq 43) as follows: $\int_{-1/2}^{1/2}\tilde{E}\,d\tilde{x} = -(1/\varphi)\int_{-1/2}^{1/2}(\partial\tilde{V}/\partial\tilde{x})\,d\tilde{x} = (\tilde{V}_{-1/2} - \tilde{V}_{1/2})/\varphi = \tilde{t}/(1+\tilde{t}) = 1$.

The second set of differential equations (eqs 41 and 42) with boundary conditions (eq 43) and initial conditions (eq 44) has been solved numerically with finite element solver software COMSOL. The steady-state solution is only dependent on the values of the φ and λ parameters. The numerical solution has been computed using over 2000 combinations of φ and λ values, covering the relevant part of the φ,λ space.

As a summary of these numerical calculations, the values of the concentration $\tilde{n}^+$ and electric field $\tilde{E}$ at both electrodes and midplane are plotted in the φ,λ space: in Figure 8 for the upper electrode, in Figure 9 for the lower electrode, and in Figure 10 at the midplane. The dotted lines indicate the applicable ranges of the five limiting cases derived in the foregoing paragraphs. Also indicated in their appropriate regimes are the analytical expressions derived for the five limiting cases.

The graphs of the numerical solutions graphically demonstrate that the assumptions made in the previous five limiting cases

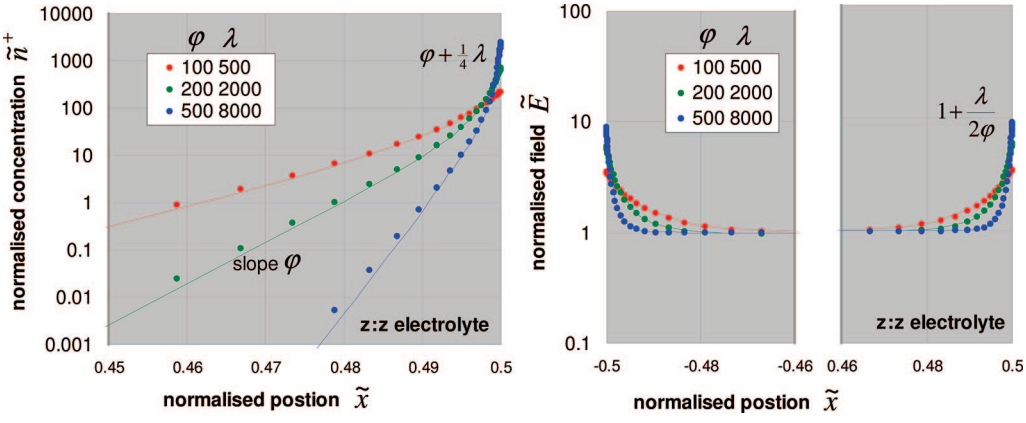

Figure 7. Concentration and field profiles for limiting case V of separated n in the range $\varphi > 10$ and $\lambda < 20\exp({}^1/_4\varphi)$. Symbols denote the numerical solution; lines denote the analytical approximations.

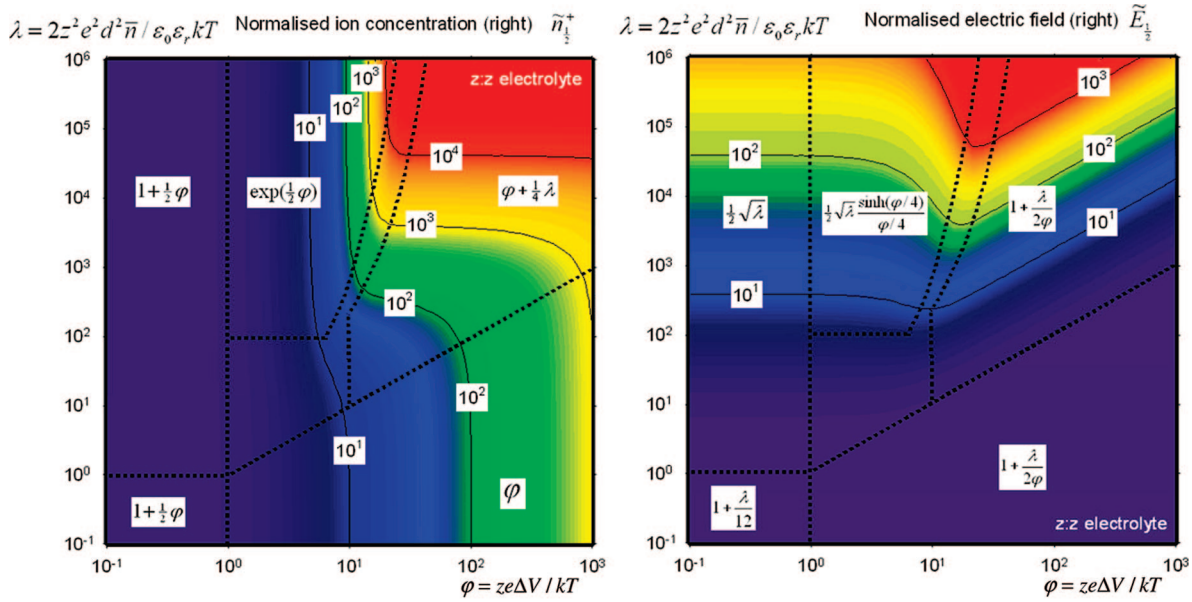

Figure 8. Numerically computed concentration $\tilde{n}^+_{1/2}$ and field $\tilde{E}_{1/2}$ at the upper electrode as function of φ and λ parameters. Also indicated are the analytical expressions and applicable ranges of the five limiting cases, previously obtained.

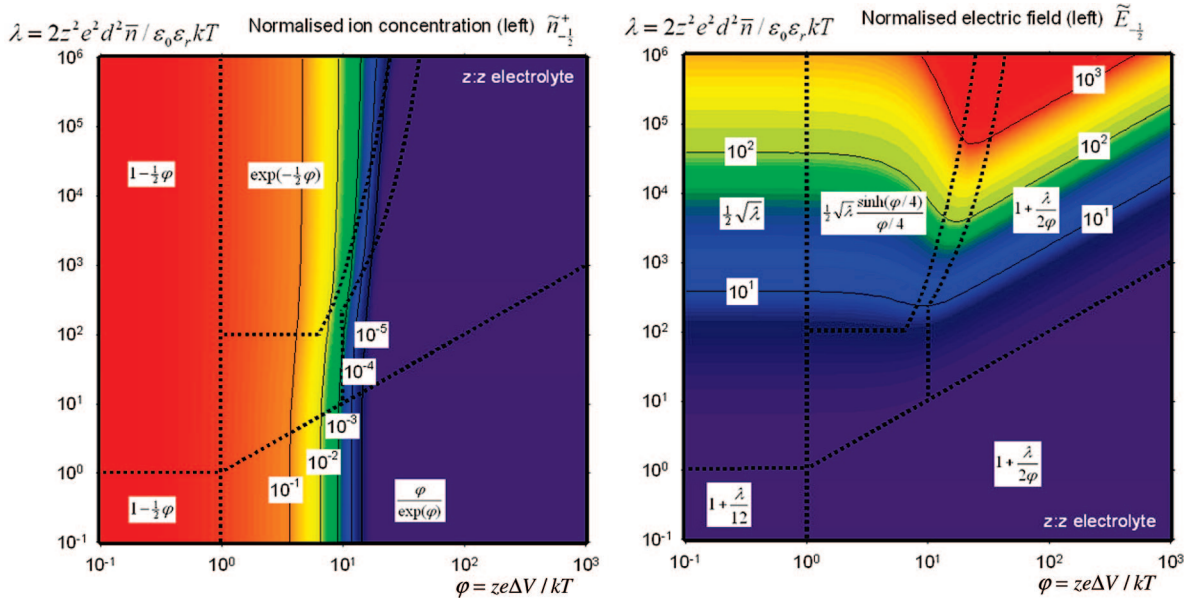

Figure 9. Numerically computed concentration $\tilde{n}^+_{-1/2}$ and field $\tilde{E}_{-1/2}$ at the lower electrode as function of φ and λ parameters. Also indicated are the analytical expressions and applicable ranges of the five limiting cases, previously obtained.

were indeed justified. First, for the limiting case II of "uniform E" in the lower right range where $\varphi > \lambda$ indeed the electric fields across the device $\tilde{E}_{1/2}$, $\tilde{E}_{-1/2}$, and $\tilde{E}_0$ are to first order all equal to unity. Analogously, for the limiting case III of "uniform n" along the left range where $\varphi < 1$, indeed the concentration across the device $\tilde{n}^+_{1/2}$, $\tilde{n}^+_{-1/2}$, and $\tilde{n}^+_0$ are to first order all equal to unity. And, in the overlapping area I "uniform n,E" of the lowerleft range $\varphi,\lambda < 1$, indeed both the field and the concentration are to first order equal to unity. Finally, for the limiting cases IV of "screened E" and "separated n", the borderline that encloses the space where $\tilde{n}_0 \approx 1$ is indeed well-approximated by $\lambda > 4\exp(^1/_2\varphi)$. And the borderline that encloses the space where $\tilde{E}_0 \approx 1$ indeed is accurately given by $\lambda < 20\exp(^1/_4\varphi)$.

Figure 11 shows a color map of the ratio between the midplane concentration and the field $\tilde{n}^+_0/\tilde{E}_0$. In red, the regime is plotted where the midplane field $\tilde{E}_0$ is multiple orders below the concentration $\tilde{n}^+_0$, corresponding to the "screened E" regime. In blue, the complementary regime is marked where the midplane concentration $\tilde{n}^+_0$ is multiple orders below the field $\tilde{E}_0$, corresponding to the "separated n" regime. Dots indicate the φ,λ values used to plot the concentration and field profiles of Figure 3 through Figure 7. Note that for high λ values the transition from the red to the blue regimes very abruptly proceeds. This means that, for microdevices with concentration and voltage values close to this transition (for instance for $\varphi = 25$ and $\lambda = 10^5$), a slight increase in voltage (to $\varphi = 50$) will have huge consequences on the concentration (4 orders decrease at the midplane) and electric field (9 orders increase at the midplane). In the next section, it will be experimentally demonstrated that this transition is real. This establishes a shortcoming of the Gouy−Chapman solution, since the latter is limited to the "screened E" regime.

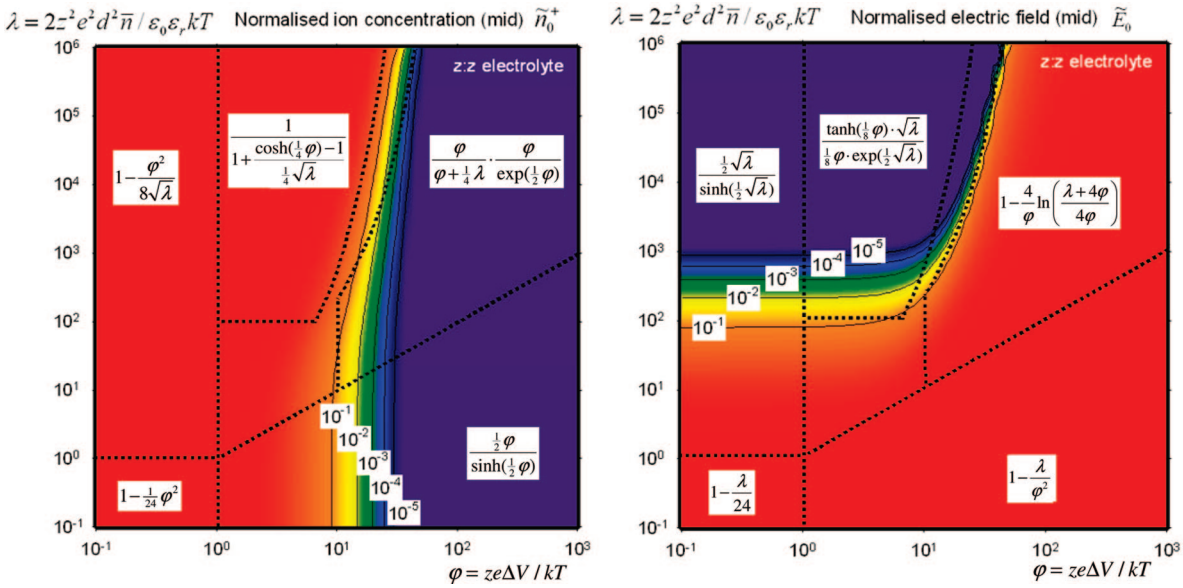

Figure 10. Numerically computed concentration $\tilde{n}_0^+$ and field $\tilde{E}_0$ at the midplane as function of φ and λ parameters. Also indicated are the analytical expressions and applicable ranges of the five limiting cases, previously obtained.

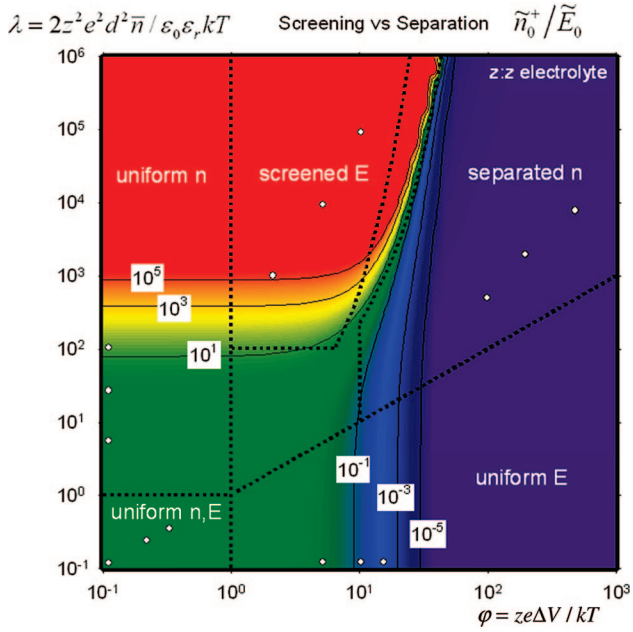

Figure 11. Overview of the regimes defined by the ratio of the midplane concentration and field.

3. Electrode Polarization Charge

To verify the theoretical results of the previous section, ideally, one would like to probe the ionic concentration and electric field profiles inside a microdevice. Unfortunately, that is not feasible, but it is possible to measure the induced charge inside the electrodes that results from the ionic concentration profile. This induced charge is referred to as "electrode polarization charge".

3.1. Theoretical Electrode Polarization Charge. Consider a parallel plate capacitor filled with a symmetrical z:z electrolyte. When both electrode plates are grounded and all positive and negative ions are distributed homogeneously between both electrode plates, then the (electronic) charge inside both electrodes is equal to zero.

Applying a potential difference ΔV between both plates introduces a charge Q_{el} inside the positive plate (and $-Q_{el}$ inside the negative plate). The magnitude of this electrode charge determines the electric field at the electrode according to Gauss' law: $Q_{el} = \varepsilon_0\varepsilon_r E_{d/2} A$. Initially, with uniform ion distribution, the electric field is uniform and equal to $\Delta V/d$. Therefore, the initial electrode charge is equal to the capacitive electrode charge $Q_0 = C_0\Delta V$, with $C_0 \equiv \varepsilon_0\varepsilon_r A/d$ the capacitance of the parallel plate device.

The initial electric field inside the capacitor will act on the ions, making their concentration and the resulting electric field profile nonuniform. Positive and negative ions will move apart and thereby reduce the electric field in the middle of the device. Since the applied potential forces the total integrated electric field over the device to remain constant, this means that the field near the electrode $E_{d/2}$ will have to increase, and hence also Q_{el}. In this electrode charge, we can distinguish a contribution due to the capacitive charge $Q_0 = C_0\Delta V$ and the remaining "electrode polarization charge" $Q_{pol} \equiv Q_{el} - Q_0$ induced by the nonuniform ion concentration profile.

There are two principal methods to calculate the theoretical value of the "electrode polarization charge". The first method is based on integrating the total external current that flows between the electrodes, as is done experimentally, starting directly after the initial capacitive charging and up to the final steady state: $Q_{pol} = \int_0^\infty I_{ext}dt$. The Ramo−Shockley[30] theorem relates the external current $I_{ext} = \sum_j z_j e(v_j/d)$ to the moving ions inside the device, as a summation over the velocities v_j of each individual ion j. Then, the "electrode polarization charge" can be rewritten as

$$Q_{pol} = \int_0^\infty I_{ext}dt = \frac{1}{d}\sum_j z_j e\left(\int_0^\infty v_j dt\right) = \frac{A}{d}\int_{-d/2}^{d/2} ze(n^+ - n^-)x\,dx \quad (45)$$

Turning to a dimensionless "polarization charge" $\tilde{Q}_{pol} \equiv (zeQ_{pol})/(kTC_0)$, this eq 45 becomes

$$\tilde{Q}_{pol} = \frac{ze}{\varepsilon_0\varepsilon_r kT}\int_{-d/2}^{d/2} ze(n^+ - n^-)x dx = \frac{\bar{n}z^2e^2d^2}{\varepsilon_0\varepsilon_r kT}\int_{-1/2}^{1/2}(\tilde{n}^+ - \tilde{n}^-)\tilde{x}d\tilde{x} = \lambda\int_{-1/2}^{1/2}\tilde{n}^+\tilde{x}d\tilde{x} \quad (46)$$

And therefore this dimensionless "polarization charge" $\tilde{Q}_{pol}$ can be calculated as the first moment of the known ionic concentration distribution.

A second and much simpler method to calculate the polarization charge is based on the electric field at the electrode $E_{d/2}$. Using the same dimensionless parameter, we obtain

$$\tilde{Q}_{pol} = \frac{ze}{kTC_0}(Q_{el} - Q_0) = \frac{ze}{kTC_0}(\varepsilon_0\varepsilon_r E_{d/2}A - C_0\Delta V) = \varphi(\tilde{E}_{1/2} - 1) \quad (47)$$

The benefit of the chosen normalization becomes clear from eq 47, because it follows that, in dimensionless terms, the capacitive part of the electrode charge $\tilde{Q}_0$ is simply equal to the voltage φ.

By using the obtained concentration and field expressions of the Gouy−Chapman solution and the five limiting cases of the complete Poisson−Boltzmann solution, both methods eq 46 and eq 47 give consistent theoretical values for the "polarization charge" $\tilde{Q}_{pol}$.

From the obtained potential $\tilde{V}$ of the Gouy−Chapman solution (eq 12), the electric field at the electrode can be determined with $\tilde{E}_{1/2} = -(1/\varphi)\cdot(\partial\tilde{V}/\partial\tilde{x})|_{\tilde{x}=1/2} = {}^1/_2\sqrt{\lambda_0}[\sinh(\varphi/4)]/(\varphi/4)$. Then, the "polarization charge" $\tilde{Q}_{pol}$ becomes $\tilde{Q}_{pol} = \varphi({}^1/_2\sqrt{\lambda_0}[\sinh(\varphi/4)]/(\varphi/4) - 1)$ with $\lambda_0 > 100$. This latter condition was established with eq 13 and eq 14. This relation is plotted in Figure 12. The Gouy−Chapman theory predicts a steep dependence on the voltage. For high voltages ($\varphi > 100$), the induced charge in the electrode would be enormous, that is, many orders of magnitude larger than the capacitive charge (equal to φ).

Also for the five limiting cases of the complete Poisson−Boltzmann solution, the polarization charge $\tilde{Q}_{pol}$ can be calculated with eq 47 combined with the obtained expressions for the field at the electrode (22, 24, 26, 31, and 37):

I. Uniform n,E: $\varphi,\lambda < 1$: $\tilde{Q}_{pol} = {}^1/_{12}\lambda\varphi$

II. Uniform E: $\varphi > 1$ and $\lambda < \varphi$: $\tilde{Q}_{pol} = \lambda/\varphi({}^1/_2\varphi/[\tanh({}^1/_2\varphi)] - 1)$

III. Uniform n: $\varphi < 1$ and $\lambda > 1$: $\tilde{Q}_{pol} = \varphi({}^1/_2\sqrt{\lambda}/[\tanh({}^1/_2\sqrt{\lambda})] - 1)$

IV. Screened E: $\lambda > 100$ and $\lambda > 4\exp({}^1/_2\varphi)$: $\tilde{Q}_{pol} = \varphi({}^1/_2\sqrt{\lambda})[\sinh({}^1/_4\varphi)]/({}^1/_4\varphi) - 1$

V. Separated n: $\varphi > 10$ and $\lambda < 20\exp({}^1/_4\varphi)$: $\tilde{Q}_{pol} = {}^1/_2\lambda$

The numerically computed electric field at the electrode (Figure 8) can be converted to the polarization charge with eq 47. This is plotted in Figure 13, together with the analytical approximations.

Comparing Figure 13 with Figure 12, it is apparent that there exists a region where the polarization charge according to the Gouy−Chapman solution agrees with the complete Poisson−Boltzmann solution. Not surprisingly, this is the region where the tacit assumption of Gouy−Chapman (zero field at the midplane) is valid, according to Figure 10: for $\lambda > 100$ and $\lambda > 20\exp({}^1/_4\varphi)$. However, in contrast to the Gouy−Chapman solution, the complete Poisson−Boltzmann solution does allow a "finite" polarization charge at high voltages ($\varphi > 100$). In addition, the complete Poisson−Boltzmann solution also exists for small concentrations ($\lambda < 100$).

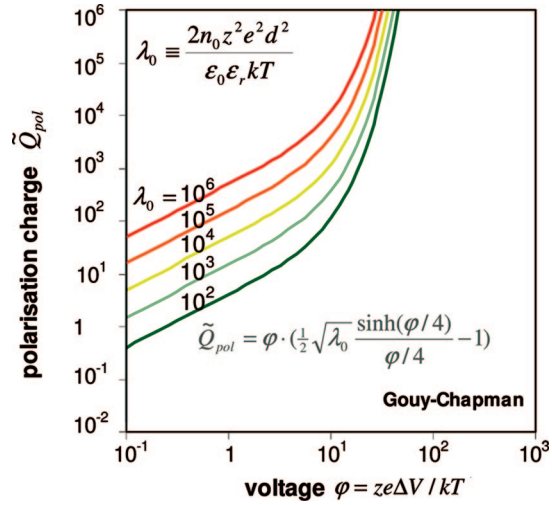

Figure 12. Calculated (dimensionless) electrode polarization charge $\tilde{Q}_{pol}$ as a function of applied (dimensionless) voltage φ, and (dimensionless) midplane concentration λ_0, with the Gouy−Chapman solution.

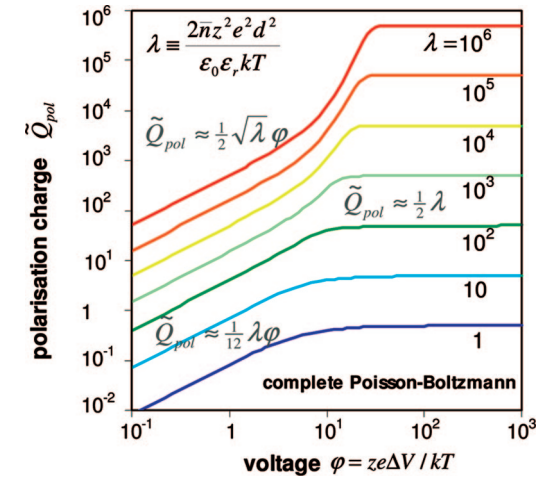

Figure 13. Numerically computed (dimensionless) electrode polarization charge $\tilde{Q}_{pol}$ as a function of applied (dimensionless) voltage φ, and (dimensionless) average concentration λ, with complete Poisson−Boltzmann solution. Also indicated are the approximations in the corresponding regimes.

3.2. Electrode Polarization Charge Measurements. Experimentally the electrode polarization charge can be determined from the transient current that flows externally between the electrodes after a voltage has been applied over the electrolyte. As a model system of a symmetrical electrolyte, we make use of a solution of polyisobutylene succinimide surfactant (OLOA 1200, Chevron) in n-dodecane (Aldrich). Electrical transient current measurements on this system have been published before.[31–34] The reason for not using a salt in water is that ion concentrations below 100 nM are inaccessible because of the autoionization of water. Pure dodecane on the other hand is a perfectly insulating liquid (bulk conductivity below 10^{-13} Ω^{-1} m^{-1}, which is 8 orders below the intrinsic conductivity of water). The OLOA surfactant (Figure 14) forms inverse micelles which acquire a univalent charge due to disproportionation[35,36] reactions. Strictly speaking, these charged inverse micelles are not ions themselves but rather contain an unbalanced amount of ions inside their polar cores. Nevertheless, we can treat these charged inverse micelles as the ion species $n^{\pm}$ of the model. As electrode devices, we use microcells made from alkali-free glass with plan-parallel ITO (indium tin oxide) electrodes coated with a 50 nm thin layer of insulating polyimide. The electrodes

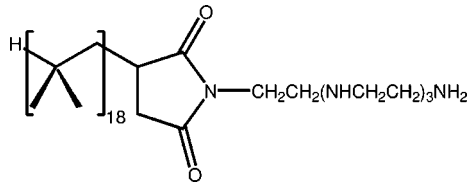

Figure 14. Chemical structure of main component of OLOA 1200.

are separated by quartz spacers with a diameter d between 4 μm and 38 μm. The overlapping electrode area is $A = 0.5$ cm^2, justifying the assumed one-dimensionality. At ambient temperature, the microcells are filled with dodecane containing up to 9 wt % of OLOA (as received).

The electrical transient current is measured with a custom-built current amplifier, specially designed for picoampere sensitivity, millisecond acquisition speed, and 6 orders dynamic range (up to microamperes). Typical transient current traces are shown in Figure 15. All transient current traces start from equilibrium (with zero voltage applied). The initial capacitive charging currents (of milliamperes during microseconds) are intentionally left out of the traces.

In this work, we are only interested in the steady-state situation, but in a related paper,[37] the time-dependence of the polarization current will also be explained using the migration-diffusion model. Here, we restrict ourselves to the time-integrated traces of the current measurements, also depicted in Figure 15. Integration is performed from 10^{-3} s onward, excluding the capacitive charging currents. After roughly 10^{-1} s, the integrated currents saturate to a final value equal to the "electrode polarization charge". This electrode polarization is measured for a range of applied voltages between 10 mV and 5 V on a series of microcells with various spacer sizes d and surfactant concentrations n_{OLOA}. Table 1 gives a representative selection from a total of 100 measurements.

By measuring the transient currents on the set of cells, integrating, and normalizing with the cell capacitance, Figure 16 is obtained. By normalizing the integrated transient current (electrode polarization charge Q_{pol}) with the cell capacitance C_0, it can conveniently be compared with the calculated dimensionless polarization charge $\tilde{Q}_{pol} \equiv zeQ_{pol}/kTC_0$. Comparing the measurement results of Figure 16 to the model calculations of Figure 12 and Figure 13, it is immediately clear that the Gouy−Chapman solution fails to describe the measurements, while the complete Poisson−Boltzmann is in excellent agreement.

The complete Poisson−Boltzmann solution, assuming a univalent electrolyte ($z = 1$) with dimensionless concentration λ as the only fit parameter is also included in Figure 16. The agreement is excellent, over 5 orders of magnitude in λ, spanning the complete range of interest. Convincingly, all three regimes of approximations $\tilde{Q}_{pol} \approx {}^1/_{12}\lambda\varphi$, $\tilde{Q}_{pol} \approx {}^1/_2\sqrt{\lambda\varphi}$ and $\tilde{Q}_{pol} \approx {}^1/_2\lambda$ can be confirmed.

As mentioned, the fits of Figure 16 are based on the assumption of a univalent electrolyte ($z = 1$). As demonstrated in Figure 17 assuming double charged ions ($z = 2$), the agreement between model and measurement deteriorates (and even more so for more highly charged ions). This demonstrates that the ions formed by the OLOA surfactant have a single charge. This can be understood, since inside low-dielectric dodecane ($\varepsilon_r = 2$), the electrostatic forces are very long-ranged, such that only ions with a size larger than the Bjerrum[18,38] diameter $d_B = z^2e^2/4\pi\varepsilon_0\varepsilon_r kT$ can withstand the neutralizing electrostatic attraction. For univalent ions, this diameter becomes $d_{B,z=1} \approx 28$ nm, for double charged ions $d_{B,z=2} \approx 112$ nm. Based on electrophoretic mobility measurements[34] on OLOA in dodecane, a diameter of 20 nm has been determined for the charged OLOA micelles, which is much too small to stabilize a double charge.

The excellent agreement in Figure 16 between the measurement results and the theory demonstrates that our solution of the Poisson−Boltzmann equation is applicable to real physical systems. This may be surprising, since the Poisson−Boltzmann equation itself is limited, in the sense that it does not take into account finite size effects and ion−ion correlations.[39] However, full Monte Carlo statistical mechanics calculations[23] on 1:1 aqueous electrolytes have shown that, up to 0.1 M concentration and 0.05 C m^{-2} electrode charge density, the Poisson−Boltzmann approach does give correct results. Our experimental results (that span the range of $\lambda < 2 \times 10^5$ and $\varphi < 200$) correspond to a maximum concentration of 4×10^{-7} M and electrode charge of 9×10^{-4} C m^{-2}, both well within the above-mentioned range of validity. So the use of the Poisson−Boltzmann equation is justified. Only our full solution to this equation can explain the measurement results; the Gouy−Chapman solution can not.

4. Discussion and Conclusions

The Poisson−Boltzmann equation is a widely applied fundament in diverse fields of colloid science, biophysics, and electrochemistry. Numerous textbooks in these fields[18–22] present the Gouy−Chapman solution as its general planar (1D) analytic solution for a symmetrical electrolyte. However, this is not fully correct. The Gouy−Chapman solution is only generally valid in the presence of a bulk electrolyte region where the electric field is zero. For macroscopic containers, this bulk electrolyte assumption is reasonable; however, for devices on the microscale, it is not. We demonstrated mathematically that for microdevices the Gouy−Chapman solution becomes restricted and even unphysical for applied voltages of more than 1 V. As an example, a recent publication[12] makes use of this bulk assumption in modeling a device (of only 300 nm size). It is found that for voltages above 0.3 V ($\varphi > 12$), impossibly high ion concentrations are obtained at the electrodes. From the present work, this can be understood as a direct consequence of the bulk assumption. Without this assumption, as can be observed in Figure 8, the ion concentration at the electrode would have been limited (to $\varphi + {}^1/_4\lambda$), even without introducing a Stern layer to account for the finite ion size.

Also in a second recent paper[34] (describing electrical measurements on OLOA in a microdevice), the Gouy−Chapman solution is used to model the polarization charge inside the diffuse double layer but failed to describe the measurements. This disagreement was falsely attributed to steric interactions of the charge carriers. In fact, the conditions of the measurements ($\lambda \approx 10^6$ and $\varphi \approx 100$) are well-inside the "separated n" regime; therefore, the bulk electric field is not zero, and the Gouy−Chapman solution is not applicable. In contrast, with the complete Poisson−Boltzmann solution (as in Figure 13), excellent agreement would have resulted.

To address these limitations of the Gouy−Chapman solution, in this work, the complete solution of the Poisson−Boltzmann equation is presented without the bulk assumption. It is mapped on the φ,λ space, defined by the dimensionless voltage $\varphi \equiv ze\Delta V/kT$ and concentration $\lambda \equiv 2\bar{n}z^2e^2d^2/\varepsilon_0\varepsilon_r kT$ parameters. It is demonstrated that the latter parameter λ (based on the average ion concentration) allows for the classification of the behavior of the system and is closely related to the conventional Debye−Hückel parameter κ (based on the bulk concentration). By numerical and analytical calculations, it is shown that for

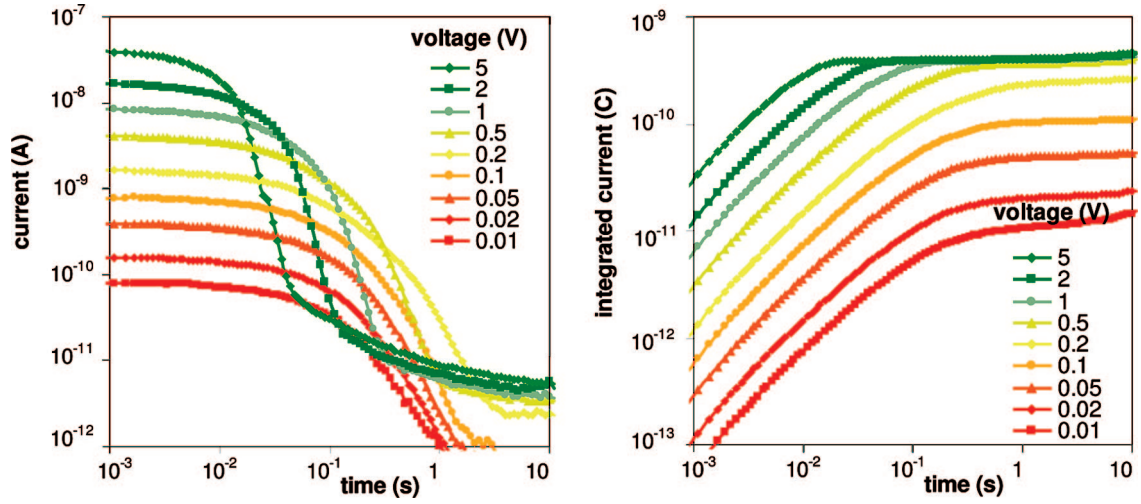

Figure 15. (left) Measured transient current as a function of applied voltage step, for 0.12 wt % OLOA in dodecane ($d = 11$ μm). (right) Time integrated current starting at 10^{-3} s.

TABLE 1: Microcell Properties

cell	d (μm)	n_{OLOA} (wt %)
1	4.0	0[a]
2	4.0	0.010
3	4.0	0.13
4	4.0	3.0
5	38	0.6
6	38	9.3

[a] A minimum electrolyte concentration was attained in cell 1 by initially filling with 4.0 wt % OLOA, purging, and finally refilling with pure dodecane. Direct attempts to reach this electrolyte concentration failed presumably because of the critical micelle concentration (estimated for OLOA as 0.005 wt %).

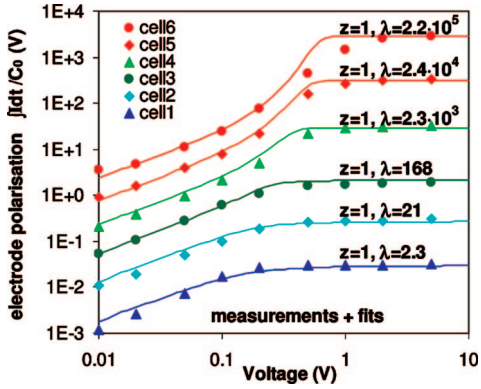

Figure 16. Measured electrode polarization (symbols) versus model (curves) based on complete Poisson−Boltzmann solution, assuming a univalent electrolyte.

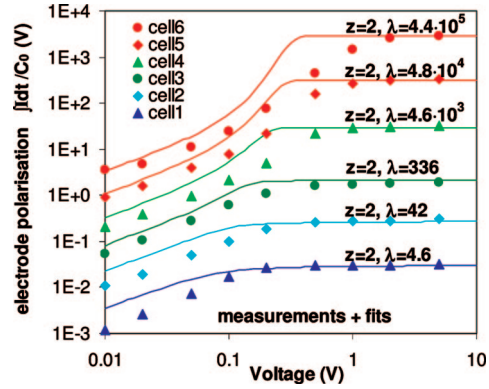

Figure 17. Measured electrode polarization (symbols) versus model (curves) based on complete Poisson−Boltzmann solution, assuming an electrolyte of double charged ions. The agreement with the measurements is not as good as that for the univalent electrolyte in Figure 16.

low voltages ($\exp(^1/_2\varphi) < ^1/_4\lambda$) the electrolyte can screen (shield) the electric field. In that case, the applied voltage is completely absorbed by the electric double layers that form at the electrodes. The characteristic size of these double layers is governed by $\lambda^{-1/2}\cdot d$ and the Gouy−Chapman solution is retrieved. However, for high enough voltages ($\exp(^1/_4\varphi) > ^1/_{20}\lambda$, order of magnitude: 1 V at micrometer scale to 5 V at macroscopic scale) we find that the positively and negatively charged species become fully separated, each at its corresponding electrode. In that case, the double layers are strongly compressed to a characteristic size of $\varphi^{-1}\cdot d$. It turns out that this compressed double layer cannot absorb the applied voltage, so away from the electrode the electric field simply becomes $\Delta V/d$.

To the best of our knowledge, this work for the first time identifies the "separated n" regime as a solution to the planar Poisson−Boltzmann equation. There have been attempts to calculate the steady-state concentration and field profiles in a planar electrolyte device, even without making the bulk assumption. In one example,[40] the numerical calculations were restricted to $\lambda < 100$ and $\varphi < 5$, which excludes the "separated n" regime. Also in more recent paper,[41] a combination of numerical and analytical solutions is presented but limited to $\varphi < 4$ and $\lambda < 400$. Consequently, the sharp transition between the "screened E" and "separated n" regimes (Figure 11) is overlooked.

In addition, we have tested our calculations against measurements of the electrode polarization charge. The electrode polarization charge on the one hand arises as a consequence of the distribution of positive and negative ions inside the electrolyte and, on the other hand, determines the electric field at the electrode−electrolyte interface. The electrode polarization charge therefore is an accessible and informative probe of the concentration and field distributions inside the electrolyte. The use of a nonaqueous apolar electrolyte allows to access low charge carrier concentrations and high voltage ranges, so that the complete range of interest could be investigated experimentally: $2 < \lambda < 2 \times 10^5$ and $0.4 < \varphi < 200$. The agreement between measurements and calculations is excellent and con-

firms the existence of a transition between low-voltage ("screened E") and high-voltage ("separated n") regimes.

This work demonstrates that an electric field can separate an electrolyte. It is interesting that recently the opposite effect has been found[42] where a separation of charged particles (due to sedimentation) generates a macroscopic electric field. Both these effects have in common that they present phenomena that add new insights to conventional wisdom in this field.

Acknowledgment. Rene van Zandwijk (Utrecht University) is acknowledged for his support in initiating the numerical calculations (formerly in Pstar). The electronic design of the transient current amplifier was made by Kees Oostveen and the assembly of the microcells was made by Els Alexander-Moonen and Gerda van de Spijker.

Supporting Information Available: An animated graph showing the ion concentration near an electrode in response to an increasing applied voltage ($\lambda = 10^5$ and $0.1 < \varphi < 1000$). The transition between the "screened E" and "separated n" regimes can clearly be observed. This material is available free of charge via the Internet at http://pubs.acs.org

References and Notes

(1) Borukhov, I.; Andelman, D.; Orland, H. *Electrochim. Acta* **2000**, *46*, 221.
(2) Boda, D.; Fawcett, W. R.; Henderson, D.; Sokolowski, S. *J. Chem. Phys.* **2002**, *116*, 7170.
(3) Biesheuvel, P. M. *J. Colloid Interface Sci.* **2001**, *238*, 362.
(4) Carnie, S. L.; Chan, D. Y. C.; Gunning, J. S. *Langmuir* **1994**, *10*, 2993.
(5) Kato, M. *J. Theor. Biol.* **1995**, *177*, 299.
(6) Forsten, K. E.; Kozack, R. E.; Lauffenburger, D. A.; Subramaniam, S. *J. Phys. Chem.* **1994**, *98*, 5580.
(7) Honig, B.; Nicholls, A. *Science* **1995**, *268*, 1144.
(8) Fogolari, F.; Brigo, A.; Molinari, H. *J. Mol. Recog.* **2002**, *15*, 377.
(9) Li, T.; Ruden, P. P.; Campbell, I. H.; Smith, D. L. *J. Appl. Phys.* **2003**, *93*, 4017.
(10) Graves, D. B.; Jensen, K. F. *IEEE Transactions on Plasma Science* **1986**, *14*, 78.
(11) Campisi, M.; Accoto, D.; Dario, P. *J. Chem. Phys.* **2005**, *123*, 204724.
(12) Lim, J.; Whitcomb, J.; Boyd, J.; Varghese, J. *J. Colloid Interface Sci.* **2007**, *305*, 159.
(13) Moya, A. A.; Castilla, J.; Horno, J. *J. Phys. Chem.* **1995**, *99*, 1292.
(14) Samson, E.; Marchand, J.; Robert, J. L.; Bournzel, J. P. *International Journal for Numerical Methods in Engineering* **1999**, *46*, 2043.
(15) Debye, P.; Hueckel, E. *Phyzik. Z.* **1923**, *24*, 185.
(16) Gouy, G. *J. de Phys.* **1910**, *9*, 457.
(17) Chapman, D. L. *Phil. Mag.* **1913**, *25*, 475.
(18) Lyklema, J. *Fundamentals of Interface and Colloid Science*; Academic Press: London, 1995; Vol. II:Solid-Liquid Interfaces.
(19) Hunter, R. J. *Foundations of Colloid Science*, 2nd ed.; Oxford University Press: New York, 2004.
(20) Bockris, J. O. M.; Reddy, A. K. N. *Modern Electrochemistry*; Macdonald: London, 1970; Vols. *1*−*2*.
(21) Bard, A. J.; Faulkner, L. R. *Electrochemical Methods: Fundamentals and Applications*, 2nd ed.; John Wiley & Sons: New York, 2000.
(22) Israelachvili, J. N. *Intermolecular and Surface Forces*, 2nd ed.; Academic Press: London, 1992.
(23) Carnie, S. L.; Torrie, G. M. *Adv. Chem. Phys.* **1984**, *56*, 141.
(24) Nernst, W. *Z. Phys. Chem.* **1888**, *2*, 613.
(25) Planck, M. *Ann. Phys. Chem.* **1890**, *40*, 561.
(26) Einstein, A. *Ann. Phys. (Leipzig)* **1905**, *17*, 549.
(27) Hsu, J. P.; Yu, H. Y.; Tseng, S. *J. Phys. Chem. B* **2006**, *110*, 25007.
(28) Hall, D. G. *J. Chem. Soc., Faraday Trans. II* **1977**, *73*, 101.
(29) Frenning, G.; Stromme, M. *J. Appl. Phys.* **2001**, *90*, 5570.
(30) Kim, H.; Min, H. S.; Tang, T. W.; Park, Y. J. *Solid-State Electron.* **1991**, *34*, 1251.
(31) Verschueren, A. R. M.; Strubbe, F.; Schlangen, L. J. M.; Neyts, K. *Proceedings of 12th International Display Workshops* **2005**, 841.
(32) Beunis, F.; Strubbe, F.; Marescaux, M.; Neyts, K.; Verschueren, A. R. M. *Appl. Phys. Lett.* **2007**, *91*, 182911.
(33) Beunis, F.; Strubbe, F.; Neyts, K.; Verschueren, A. R. M. *Appl. Phys. Lett.* **2007**, *90*, 182103.
(34) Kim, J.; Anderson, J. L.; Garoff, S.; Schlangen, L. J. M. *Langmuir* **2005**, *21*, 8620.
(35) Morrison, I. D.; Ross, S. *Colloidal Dispersions: Suspensions, Emulsions and Foams*; John Wiley and Sons: New York, 2002.
(36) Strubbe, F.; Verschueren, A. R. M.; Schlangen, L. J. M.; Beunis, F.; Neyts, K. *J. Colloid Interface Sci.* **2006**, *300*, 396.
(37) Beunis, F.; Strubbe, F.; Marescaux, M.; Beeckman, J.; Neyts, K.; Verschueren, A. R. M. *Phys. Rev. E* **2008**, *78*, 11502.
(38) Bjerrum, N. *Kgl. Danske Videnskab. Selskab. Math.-fys. Medd.* **1926**, *7*, 1.
(39) Forsman, J. *J. Phys. Chem. B* **2004**, *108*, 9236.
(40) Franceschetti, D.; Macdonald, J. *J. Appl. Phys.* **1979**, *50*, 291.
(41) Bazant, M.; Thornton, K.; Ajdari, A. *Phys. Rev. E* **2004**, *70*, 21506.
(42) Rasa, M.; Philipse, A. P. *Nature* **2004**, *429*, 857.

JP800675W